

Experimental Demonstration of Three-Photon Coherent Population Trapping in an Ion Cloud

M. Collombon, C. Chatou, G. Hagel, J. Pedregosa-Gutierrez, M. Houssin, M. Knoop, and C. Champenois[✉]

PIIM, Aix-Marseille University and CNRS, 13397 Marseille cedex 20, France

(Received 11 March 2019; revised manuscript received 18 June 2019; published 18 September 2019)

An interrogation protocol based on coherent population trapping in an N -level scheme atomic system leads to dark resonances involving three different photons. An ensemble of several hundred radio-frequency-trapped Ca^+ ions is probed by three lasers simultaneously locked onto the same optical frequency comb, resulting in high-contrast spectral lines referenced to an atomic transition in the terahertz domain. We discuss the cause of uncertainties and limitations of this method and show that reaching subkilohertz resolution is experimentally possible by this interrogation protocol.

DOI: 10.1103/PhysRevApplied.12.034035

The quantum interference between two excitation paths that is responsible for coherent population trapping (CPT) is an example of a quantum effect based on atomic coherence [1]. When this interference occurs in a Λ -scheme atomic system, the atomic population is trapped in a coherent superposition of the two ground substates, dressed by the coupling photons. If the two ground dressed substates are stable, the excited state is no longer populated. This population trapping can be observed by a dark resonance in the fluorescence signal [2] or by the cancellation of the laser absorption [3]. Two-photon CPT has proven its relevance as a resource for high-precision measurement in magnetometry [4,5] and in the so-called CPT microwave clock, where no microwave cavity is needed [6–8]. The best reported performances concerning short-term stability are reached with a vapor-cell clock with fractional frequency stability of a few $10^{-13}/\sqrt{\tau}$ [9,10]. Cold-atom clocks are expected to perform better with regard to long-term stability, and instability on the order of 3×10^{-13} after an averaging time of 1 h was reported in Ref. [11]. In this paper, we report the observation of a three-photon CPT in a cold cloud of trapped ions and discuss the main causes of the shift and broadening.

In CPT microwave clocks, two phase-coherent lasers perform optical spectroscopy of the gigahertz transition between hyperfine sublevels of the heaviest alkali metals Rb and Cs. When the laser-frequency difference matches the ground-state splitting, the atomic population is trapped in a dark state and the optical signal is used to reference this frequency difference to the gigahertz transition. Sub-Doppler-spectroscopy is performed by exploiting the Lamb-Dicke effect [12], which

provides a first-order Doppler cancellation whenever the displacement of the absorbers over successive excitations is smaller than $\lambda/(2\pi)$, where λ is the transition wavelength and is on the order of centimeters for microwave transitions and micrometers for optical transitions. Experimental results in room-temperature cells where the atom mean free path is reduced to the millimeter scale by filling them with buffer gas or by scaling the cell size to millimeter scale prove that the Lamb-Dicke regime can be reached for microwave transitions even if they are excited by means of two lasers operating in the optical range. The contrast of the dark line is then limited by the relaxation of the coherence between the two substates. It can be induced by the collisions of the atoms with the buffer gas and/or the cell glass [13] and by the noise on the relative phase between the optical fields [11,14].

We investigated in Ref. [15] a three-photon CPT that occurs in a four-level atomic system with an N -shaped laser-interaction scheme, where three of the four states involved are stable or metastable. Extension from two to three lasers involved in the dark-resonance condition allows the cancellation of the first-order Doppler effect by a geometric phase matching of the three laser wave vectors [16–20], simulating a Lamb-Dicke effect with an effective infinite wavelength. This example of an N -level scheme can be found in the heaviest alkaline-earth-metal ions Ca^+ , Sr^+ , and Ba^+ [15] and in neutral alkaline-earth-metal atoms such as Sr and Yb [20]. We report here the observation of a three-photon dark resonance in a cloud of Ca^+ ions stored in a linear quadrupole trap and laser-cooled by Doppler laser cooling. In this ion, the three optical fields required to build the coherent dark state lie in the optical and near-infrared domain, spanning more than one octave. Therefore, their phase coherence is ensured by an ultrastable laser through a simultaneous lock on an optical

* caroline.champenois@univ-amu.fr

frequency comb (OFC) [21,22]. The dark-resonance condition defines a combination of the three optical frequencies, which is referenced to a magnetic dipole transition at 1.82 THz.

In the following, we first present the experimental conditions for observing a three-photon dark resonance in the fluorescence of a cloud of trapped ions. We review the major effects that contribute to the linewidth, frequency shift, and contrast of the dark line: the Doppler effect, the Zeeman effect, and power-induced effects.

I. CONDITIONS FOR OBSERVATION OF A THREE-PHOTON CPT

The three-photon dark line is observed in the laser-induced fluorescence emitted by a cloud of $^{40}\text{Ca}^+$ ions stored in a linear quadrupole rf trap. The calcium ions are Doppler-laser-cooled on their (E1) resonance transition $4S_{1/2} \rightarrow 4P_{1/2}$ at 396.85 nm (label *B*). This transition is not closed, and once in the $4P_{1/2}$ excited state, the ions can decay to the metastable $3D_{3/2}$ state with probability $\beta = 0.064$ [23]. Keeping the ions within the cooling cycle thus implies the use of a second “repumping” laser, tuned to the (E1) dipole transition $3D_{3/2} \rightarrow 4P_{1/2}$ at 866.21 nm (label *R*). The third laser involved in the CPT process is resonant with the (E2) electric quadrupole transition $4S_{1/2} \rightarrow 3D_{5/2}$ at 729.15 nm [label *C*, see Fig. 1(a) for the transition scheme].

Because it is based on the second-order expansion of the interaction Hamiltonian, this last transition has a typical coupling strength that is 8 orders of magnitude smaller than the ones induced on the dipole transitions involved

in the laser cooling [24]. Despite the weakness of the laser-atom interaction on this transition, it can play a major role in the internal state dynamics provided that a resonance condition is fulfilled [15]. By a partial diagonalization of the system, this condition can be extrapolated from two-photon Λ -scheme dark resonances [1] and is given by

$$\Delta_R = \Delta_B - \Delta_C - \delta_C, \quad (1)$$

where Δ_R , Δ_B , and Δ_C are the one-photon detunings of the three lasers and δ_C is the light shift induced by the quadrupole coupling on the 729-nm transition [15] (see the Appendix). The trapping state is a coherent superposition of the three stable and metastable dressed states that is not coupled by laser excitation, and once trapped in this state, the ions do not emit any photons.

When fulfilled, the three-photon resonance condition implies a strong relation between the three laser frequencies:

$$\omega_R + \omega_C - \omega_B + \delta_C = \omega_{\text{THz}}, \quad (2)$$

where ω_{THz} is the frequency of the magnetic dipole transition between $3D_{3/2}$ and $3D_{5/2}$, which appears as the reference transition. The frequency ω_{THz} is 1.82 THz in Ca^+ , and its absolute value is known with ± 8 -Hz uncertainty through Raman spectroscopy on a single trapped ion [25,26]. For the typical intensity and detuning of the laser at 729 nm, δ_C is below 100 Hz and can be ignored in the results reported in the following.

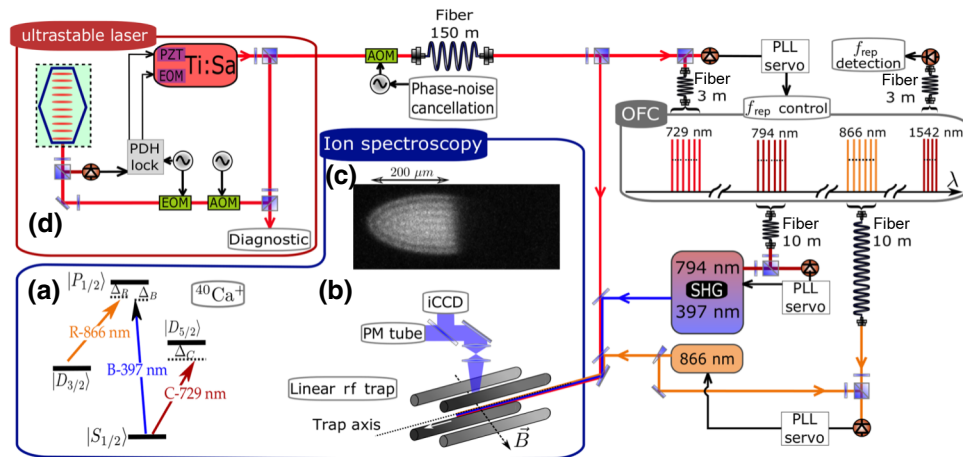


FIG. 1. (a) Transition scheme for the three-photon CPT in Ca^+ . (b) The experimental setup: the three laser beams propagate along the trap symmetry axis, the linear radio-frequency trap is represented by its four rods, and the laser-induced fluorescence is recorded by a photomultiplier (PM) tube for photon counting and a intensified CCD (iCCD) camera for spatial resolution of the fluorescence. (c) A cloud made of 710 (± 35) ions. The ions shelved in the metastable $D_{5/2}$ state or trapped in the coherent superposition are dark and split from the bright ions because they do not feel the radiation pressure induced by the cooling laser on the bright ions. (d) Setup for the laser phase lock, based on an OFC locked onto an ultrastable Ti:sapphire (Ti:Sa) laser. AOM, acousto-optic modulator; EOM, electro-optic modulator; PDH, Pound-Drever-Hall; PLL, phase-locked loop; SHG, second-harmonic generation.

In the experiments presented here, the beams of the three lasers copropagate along the symmetry axis of a linear quadrupole rf trap [see Fig. 1(b)] and the effective wave vector $\Delta \vec{k}$ controlling the first-order Doppler effect on the dark line is that of the magnetic dipole transition $k_{\text{THz}} = 2\pi/\lambda_{\text{THz}}$, where λ_{THz} is the $3D_{3/2}-3D_{5/2}$ transition wavelength, equal to $165\ \mu\text{m}$. The quadrupole trap is described in Refs. [27,28]. Its main characteristics are an inner radius of $3.93\ \text{mm}$ for a rod radius of $4.5\ \text{mm}$ [29] and an rf trapping frequency of $5.2\ \text{MHz}$. For the work presented here, it is operated with a peak-to-peak rf-voltage difference between neighboring rods of $826\ \text{V}$ (Mathieu parameter $q_x = 0.24$) and a cloud contains a few tens to thousands of ions. The Doppler laser cooling drives the ion cloud from a gas, through the liquid phase, to a crystal phase [30], with a temperature estimated to be on the order of $10\ \text{mK}$. Once in the liquid and crystal phases, the ion cloud forms an ellipsoid [31,32] with a diameter ranging from 80 to $280\ \mu\text{m}$ and a length ranging from 120 to $740\ \mu\text{m}$ for a number of ions between 40 and 2750 [see Fig. 1(c)]. The $397\text{-}\text{nm}$ and $866\text{-}\text{nm}$ lasers have an elliptical cross section, with an aspect ratio of 2 and a mean squared diameter at the position of the cloud of 4.0 and $4.7\ \text{mm}$, respectively. The laser intensity and wave vectors can be considered uniform all over the ion cloud. The $729\text{-}\text{nm}$ laser has the smallest beam size, with a waist diameter of $300 \pm 20\ \mu\text{m}$. It is still larger than the largest of the cloud diameters but its intensity is not uniform over the largest clouds. Keeping all the atoms inside the three laser beams cancels any broadening induced by the finite interaction time due to atom motion, which is an identified cause of broadening of two-photon CPT lines when observed for an atomic beam or a gas in a cell [7,33,34].

For the observation of the dark lines, the three lasers are applied continuously on the cloud. As is well known for two-photon CPT, the stability of the phase relation between the three dressing lasers is mandatory to reach a stationary dark state. For that purpose, we use a commercial OFC to transfer the phase stability between the three lasers [22]. We take advantage of an ultrastable laser at $729\ \text{nm}$ (relative Allan variance of 10^{-14} at $1\ \text{s}$) to serve as a local reference for the offset-free OFC, produced by frequency difference in a nonlinear crystal (TOPTICA DFC CORE+). The OFC repetition rate f_{rep} is $80\ \text{MHz}$ and three dedicated coherent outputs at 729 , 794 , and $866\ \text{nm}$ allow three simultaneous phase locks (the $397\text{-}\text{nm}$ radiation is produced by second-harmonic generation). The OFC is first locked onto the $729\text{-}\text{nm}$ laser by a phase-locked loop with use of the beat signal of the ultrastable laser and the closest comb eigenmode. Then the 794 - and $866\text{-}\text{nm}$ lasers are locked onto the OFC by the same technique, but in this case feedback is applied to the lasers. Their frequency measurement requires identification of the indices N_B , N_R , and N_C of their closest eigenmode emitted by the OFC and measurement of the relative value of the laser

frequency compared with this eigenmode, which is bound by $\pm f_{\text{rep}}/2$. The indices N_B , N_R , and N_C are determined without ambiguity with the help of a wavemeter with an accuracy of $\pm 10\ \text{MHz}$. The uncertainty on each laser-frequency measurement lies in the kilohertz range and is $N_B \times \sigma_{\text{rep}}$, $N_R \times \sigma_{\text{rep}}$, or $N_C \times \sigma_{\text{rep}}$, where σ_{rep} is the uncertainty of the repetition rate, equal on average to $1.5\ \text{mHz}$ (one standard deviation). The resulting uncertainty on the deduced terahertz frequency is given by $(N_B - N_R - N_C) \times \sigma_{\text{rep}}$, which is on the order of $34\ \text{Hz}$, 2 orders of magnitude lower than the optical frequency uncertainty.

Spectra are observed while we collect the photons emitted at $397\ \text{nm}$ on the $4P_{1/2} \rightarrow 4S_{1/2}$ transition while the frequency of the R laser is scanned. Typical laser powers are $10\text{--}20\ \text{mW}$ at $397\ \text{nm}$ (P_B), $0.5\text{--}5\ \text{mW}$ at $866\ \text{nm}$ (P_R), and $5\text{--}25\ \text{mW}$ at $729\ \text{nm}$ (P_C). The width of the complete spectrum is greater than $100\ \text{MHz}$; Fig. 2 shows a portion of such a spectrum, selected around the three-photon resonance condition as given by Eq. (1). By comparing the two plots in Fig. 2, showing the fluorescence signal with and without the C laser exciting the weak transition, one can deduce that some ions are “shelved” in the metastable $D_{5/2}$ state [35], independent of any resonance condition. The narrow features superimposed on the reduced signal (blue line) are the signature of the three-photon CPT. They correspond to the trapping of a fraction of the ions from the cooling cycle to the dark state. With the detection scheme chosen, it is not possible to quantify the number of ions transferred from the metastable state to the dark state. More than half of the ions remain bright and thus are laser-cooled. By sympathetic cooling of the dark atoms [36], the ion cloud remains in a liquid phase throughout the complete frequency scan, even though the radiation pressure is responsible for spatial separation of the bright and dark

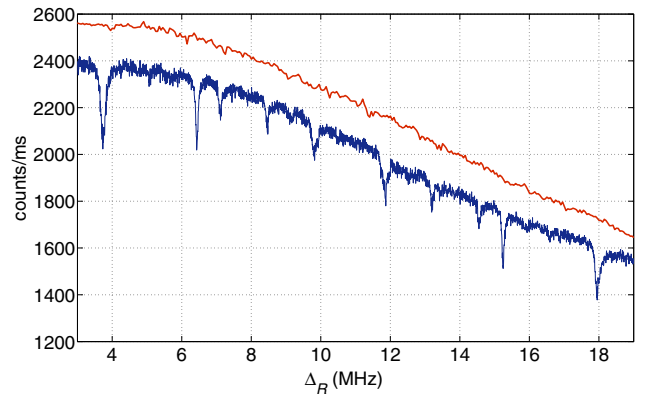


FIG. 2. Laser-induced fluorescence of a cloud of 560 ± 25 laser-cooled ions versus the detuning of the repumping R laser for $\Delta_B = -25.8\ \text{MHz}$ and $\Delta_C = -36.3\ \text{MHz}$. The top curve shows photon counts when the cooling and repumping lasers are *on* ($P_B = 10\ \text{mW}$, $P_R = 1\ \text{mW}$). For the lower curve, the $729\text{-}\text{nm}$ laser is also applied ($P_C = 12.1\ \text{mW}$). The background is 570 ± 25 counts/ms.

ions [see Fig. 1(c)]. This sympathetic cooling offers the great advantage of keeping constant the number of ions inside the laser beam during the whole recording.

The splitting of the dark line into several pairs of lines is due to the local magnetic field, which lifts the degeneracy of the Zeeman substates. A magnetic field on the order of 1 G is applied, and the three laser polarizations are linear, perpendicular to the trap axis, and nearly perpendicular to the local magnetic field. We label each transition by a number m_{THz} according to its Zeeman shift on the terahertz transition frequency $\delta_Z(m_{\text{THz}}) = m_{\text{THz}}\mu_B B$. With $g_{3/2}$ and $g_{5/2}$, the Landé factors of the $D_{3/2}$ and $D_{5/2}$ states, and $m_J(D_{3/2})$ and $m_J(D_{5/2})$, the Zeeman substates involved in the transition, $m_{\text{THz}} = g_{5/2}m_J(D_{5/2}) - g_{3/2}m_J(D_{3/2})$. Table I provides the transitions based on the largest couplings (quantified by their relative Rabi frequencies) imposed by the chosen laser polarization relative to the local magnetic field and controlled by the selection rules of electric dipole (E1) and electric quadrupole (E2) transitions [37]. The stability of the center frequency of each line is limited by the long-term fluctuations (more than 100 s) of the local magnetic field, which is measured to be 0.4 mG (peak to peak). It contributes an uncertainty proportional to m_{THz} and on the order of 1 kHz. The short-term fluctuations of the total local magnetic field are measured to be 6 mG (peak to peak) and are responsible for an m_{THz} -dependent broadening on the order of 20 kHz (peak to peak). The Doppler effect on the three-photon dark lines is 415 times smaller than the Doppler effect on the optical cooling transition at 397 nm. It broadens the three-photon dark lines by 20 kHz (FWHM) for a sample at 10 mK. In the spectrum in Fig. 2, the measured linewidths range from 42 to 218 kHz.

II. DEMONSTRATION OF THE THREE-PHOTON RESONANCE CONDITION

To prove that these extra lines result from the three-photon process and are referenced to the terahertz

TABLE I. Zeeman substates of the two metastable states giving rise to the observed terahertz transitions. The corresponding terahertz transitions are labeled by the number m_{THz} , defined by the Zeeman shift $\delta_Z(m_{\text{THz}}) = m_{\text{THz}}\mu_B B$ (for the labeling only, m_{THz} is rounded in the assumption of a Landé g factor equal to 2 for the electron). $\overline{\Omega}_C$ and $\overline{\Omega}_R$ are the Rabi frequencies relative to the Rabi frequency for $m_{\text{THz}} = \pm 21/5$. All the transitions share the same Rabi frequency on the B transition.

$m_J(D_{3/2})$	$m_J(D_{5/2})$	m_{THz}	$\overline{\Omega}_C$	$\overline{\Omega}_R$
$\mp 3/2$	$\pm 5/2$	$\pm 21/5$	1	1
$\pm 1/2$	$\pm 5/2$	$\pm 13/5$	1	$1/\sqrt{3}$
$\mp 1/2$	$\pm 3/2$	$\pm 11/5$	$1/\sqrt{5}$	$1/\sqrt{3}$
$\pm 1/2$	$\pm 3/2$	$\pm 7/5$	$1/\sqrt{5}$	$\sqrt{2/3}$
$\pm 3/2$	$\pm 3/2$	$\pm 3/5$	$1/\sqrt{5}$	1

transition, we focus on the dark line defined by $m_{\text{THz}} = -13/5$ because of its high contrast. The R -laser frequency ω_R is scanned for different values of ω_C in an interval of 16 MHz, while ω_B is kept constant. The frequency step is 1 kHz and signal is accumulated for 150 ms at each step. Each scan is performed four times and the data are averaged. Each observed line profile is fitted to a Lorentzian profile and the center of the line ω_R^c has an uncertainty on the order of 1 kHz (1σ) conditioned by the frequency step and the signal-to-noise ratio. The frequency combination $\Delta_{RCB} = \omega_R^c + \omega_C - \omega_B$ is expected to give access to the magnetic dipole transition frequency, once the experimental shifts are removed, the Zeeman shift being the largest one identified. As some non-negligible light-induced effects also shift the dark lines, and their dependence on the m_{THz} number is not known, we do not use the average frequency of the $+m_{\text{THz}}$ and $-m_{\text{THz}}$ lines to deduce the unshifted frequency. We rather estimate the local magnetic field by using several multiline spectra such as the spectrum in Fig. 2 and adjusting the linear fit of the dark-resonance frequencies $\omega_R^c(m_{\text{THz}})$ with the m_{THz} values (see Fig. 3, where they are plotted with respect to the transition frequency $\omega_{P_{1/2}D_{3/2}}$ reported in Ref. [38]). The Zeeman shift $\delta_Z(-13/5)$ of the $m_{\text{THz}} = -13/5$ dark line is evaluated with an uncertainty of ± 6 kHz dominating the total uncertainty of the terahertz frequency. As shown in Fig. 4, the Zeeman-corrected transition frequencies do not exactly match the $3D_{3/2}$ - $3D_{5/2}$ transition frequency f_{DD} in Ref. [26] and are shifted from this reference value by $\delta f = \Delta_{RCB} - \delta_Z(-13/5) - f_{DD}$, corresponding to between +5 and -15 (± 6) kHz. These shifts are 3 orders of magnitude smaller than the range covered by the one-photon detuning Δ_R , and we consider that the three-photon resonance condition is demonstrated. Nevertheless, their plot against the $m_{\text{THz}} = -13/5$ transition detuning $\Delta_R^Z = \omega_R^c - \omega_{P_{1/2}D_{3/2}} + \delta_R^Z(-13/5)$, where $\delta_R^Z(-13/5)$ is the Zeeman shift on the R transition, shows a correlation between the

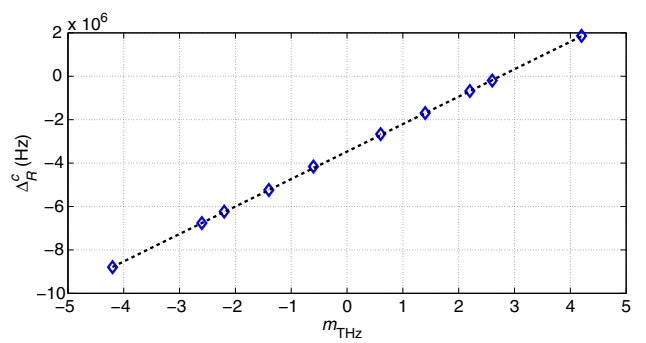


FIG. 3. Dark-resonance frequency $\omega_R^c(m_{\text{THz}})$ of several Zeeman transitions versus their corresponding m_{THz} value. The frequencies are plotted as detunings $\Delta_R^c(m_{\text{THz}})$; see the text for details. The black line is the linear fit used to calculate the average magnetic field seen by the ions.

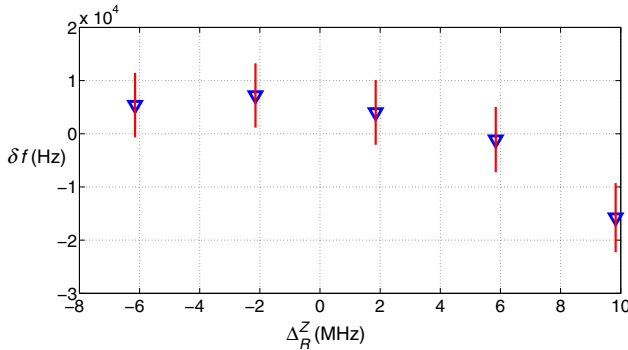


FIG. 4. Frequency shift δf on the 1.82-THz transition for the $m_{\text{THz}} = -13/5$ dark line observed for five different sets of $\{\omega_C, \omega_B\}$ versus the one-photon detuning Δ_R^Z that fits the three-photon resonance condition. The Zeeman effect is removed from the shift and is added to the measured one-photon detuning for the Zeeman-shifted R transition (Eq. 1). $P_B = 10$ mW, $P_R = 2$ mW, $P_C = 8$ mW, and $\Delta_B = -24.94$ MHz. The error bars correspond to ± 1 standard deviation.

shifts and the detunings that cannot be explained by any drifts in the experimental setup or by the coupling on the quadrupole transition δ_C . Dependence of the light-induced shift on the one-photon detuning is observed in two-photon CPT for continuous laser excitation [7,34,39] and with a Ramsey interrogation scheme [14,40]. When they are no light shifts induced by neighbor transitions, they are understood as induced by the relaxation of the coherence between the stable and metastable states involved in the dark state. This relaxation can be due to collisions but is most probably due to laser relative phase diffusion in our cold-atom system in an ultrahigh vacuum (with a pressure lower than 10^{-9} mbar). In the case of the three-photon CPT, the only light shifts that can be responsible for a dark-line frequency shift are the ones shifting the $3D_{3/2}$ or the $3D_{5/2}$ Zeeman substates, as the other ones cancel in the three-photon resonance condition (Eq. 1).

III. POWER-INDUCED SHIFTS

In the case of a three-photon CPT, interpreted as a laser-mediated Λ scheme [15], the relevant one-photon detuning is Δ_R and the laser couplings on the two arms of the Λ scheme are dominated by the laser excitation on the R transition. This description of the N -level scheme is relevant for a sufficiently strong coupling on the weak C transition. This is confirmed by the results reported in Fig. 5, where, contrary to a conventional light-shift effect, it takes a minimum laser power P_C for the frequency shift to reach a value independent of this power. This behavior is attributed to an ineffective Λ scheme when the coupling on the quadrupole transition is too weak.

The dependence of the frequency shift on the power of the R laser is shown in Fig. 6 for the $m_{\text{THz}} = -13/5$ line.

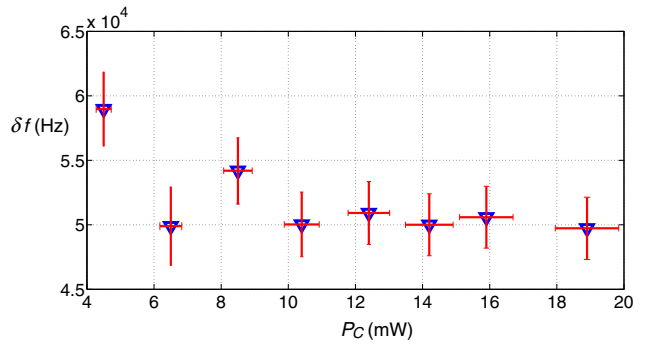


FIG. 5. Frequency shift of the Zeeman subtransition $m_{\text{THz}} = -13/5$ versus P_C , the laser power on the quadrupole transition, for one-photon detuning $\Delta_R^Z = -10.6$ MHz. The other laser powers are $P_B = 10$ mW and $P_R = 1$ mW.

The results show a linear behavior of δf with P_R , which can be extrapolated for $P_R = 0$ to 6.0 ± 3.4 kHz, showing that other experimental parameters are also responsible for shifts. In the case of the $m_{\text{THz}} = -13/5$ line, a light-shift effect can be induced by a small projection of the R -laser polarization along the magnetic field axis, which then couples the $3D_{3/2}$, $m = -1/2$ substate to the $4P_{1/2}$, $m = -1/2$ substate. The light shift induced by the far-detuned R couplings to the $4P_{3/2}$ state is estimated to be less than 10 Hz. In the range of the parameters used to observe the three-photon dark line, no significant dependence of the frequency shifts on the laser power P_B are observed for power ranging from 5 to 20 mW. Other kinds of power-induced shifts have been identified in a two-photon CPT clock [39,41]. They are due to the relaxation of the coherence between the stable and metastable states involved in the dark state and are proportional to the one-photon detuning. This extra effect certainly contributes to the total power-induced shift because of the finite phase coherence of the three lasers [21,22].

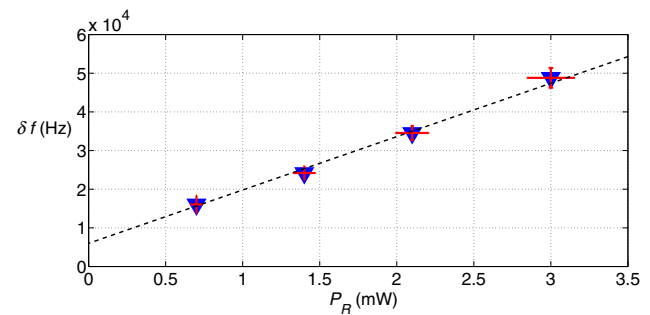


FIG. 6. Frequency shift of the Zeeman subtransition $m_{\text{THz}} = -13/5$ measured for different R -laser powers P_R (blue dots) and for an effective one-photon detuning $\Delta_R^Z = -7.74$ MHz. The dark line is a linear fit of this plot, with slope 13.8 ± 1.8 kHz/mW and limit shift for null power P_R equal to 6.0 ± 3.4 kHz (1σ). The other laser powers are $P_B = 19$ mW and $P_C = 10.4$ mW.

IV. METROLOGICAL PERFORMANCE

To quantify the metrological performance of the three-photon CPT dark line as a terahertz reference, we assume these shifts are under control and focus on the linewidth, the absolute signal level, and the contrast of the dark line. We recall that in the present experimental setup, each line is broadened by a residual Doppler effect (estimated to a minimum of 20 kHz FWHM) and by a fluctuating Zeeman effect (estimated to be $8.4 \times m_{\text{THz}}$ kHz peak to peak). Furthermore, in the range of our experimental parameters, the observed power-induced broadening is due to the coupling only on the R transition. The narrowest observed dark lines (linewidth of 45 kHz for $P_R = 0.7$ mW) are the ones with the smallest coupling on the R transition, identified by $|m_{\text{THz}}| = 11/5$ and $13/5$ (see Table I). The maximum dark-line contrast, reaching 25%, is observed for the lines $|m_{\text{THz}}| = 13/5$ and $21/5$, and they are the ones with the largest coupling on the C transition. These two independent conditions point to $|m_{\text{THz}}| = 13/5$ as the transition with the best contrast-to-broadening ratio in the context of our present experimental setup.

In Fig. 7, we plot the linewidth and contrast of the $m_{\text{THz}} = -13/5$ dark line for the five different sets of $\{\omega_C, \omega_B\}$, as observed for Fig. 4. The data show a dependence of the linewidth and contrast on the one-photon detuning Δ_R^c for which the CPT occurs while all the laser powers are kept constant. We think that this effect can be explained by the relative position of the dark line in the broader fluorescence spectral profiles of the trapped ions, due to competition with the strong transitions involved in laser cooling. Further studies are required to identify the best condition to reach the large contrast and small linewidth optimum, but these curves provide very positive perspectives as we find in the same detuning range the smallest shifts, the largest contrast, and the narrowest linewidth.

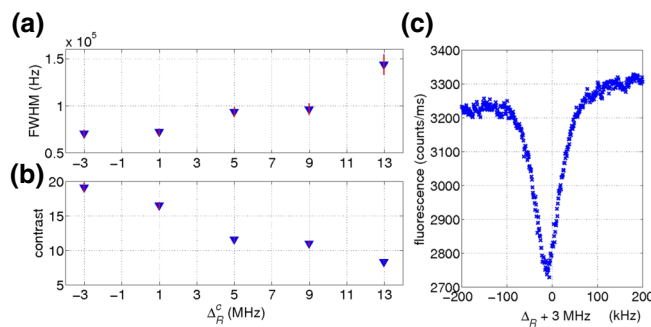


FIG. 7. FWHM (a) and contrast (b) of the $m_{\text{THz}} = -13/5$ dark line observed for five different sets of $\{\omega_C, \omega_B\}$ versus Δ_R^c ; same experiments as for Fig. 4. (c) Line profile of the dark line showing the largest contrast and the smallest linewidth of these five observations. The background induced by stray light is 520 ± 25 counts/ms.

Considering that the Doppler broadening can be canceled if the phase-matching condition $\vec{k}_B - \vec{k}_R - \vec{k}_C = \vec{0}$ is obeyed [18] or alternatively by a Lamb-Dicke effect on the terahertz transition wavelength scale [42], the signal-to-noise ratio could be increased with a larger number of ions building the dark line. If the size of the cloud is expanded, the position-dependent systematic shifts are expected to broaden the spectroscopic lines [43–45]. Nevertheless, when varying the number of trapped ions from 60 to 400, with all other parameters fixed, we observe no variation of the terahertz-frequency shift or of the dark-line width within the 6-kHz resolution.

As the magnetic field fluctuations can be actively reduced by a factor 50 and the sensitivity to these fluctuations can also be reduced by use of the transitions $m_{\text{THz}} = \pm 1/5$ if other laser-polarization and laser-propagation directions are permitted by the setup, a linewidth in the kilohertz range, or lower, together with a large contrast, seems to be very accessible. It would enable one to identify effects that are so far too small to be detected and to access resolution on the order of 10^{-9} , which is the state of the art in terahertz precision spectroscopy [42,46]. Indeed, in a system without any experimentally induced decoherence, one can show that subkilohertz linewidths can be observed [18]. Furthermore, with 25% contrast and an average fluorescence signal of 4000 counts/ms, which is typical for the fluorescence of 1000 trapped ions in the optimum conditions for a narrow dark line, the signal-to-noise ratio at 1 ms reaches 16. Even with a kilohertz linewidth, such a large signal-to-noise ratio allows the resolution to be increased to the order of 10^{-11} by averaging data over seconds.

V. CONCLUSION

The demonstrated three-photon CPT has great potential for high-resolution spectroscopy. Very similar to two-photon CPT, the interrogation protocol depends on numerous parameters that have to be further explored. In two-photon CPT, they are strongly mitigated by the use of a Ramsey-type pulsed protocol [47,48], and use of a pulsed interrogation method for the three-photon CPT is certainly a route to be tested. The originality of our approach allows us to access the terahertz domain, an insufficiently explored and very promising spectral domain, so far associated with rotational transitions in light molecules. Although the production of continuous-wave terahertz radiation from the three optical radiations involved is still an issue, this configuration could be of use to transmit the 1.82-THz reference signal by optical means and to benefit from very efficient detectors. Indeed, because terahertz radiation hardly propagates over long distances in air, its phase-coherent transfer implies coherent duplication of its phase information onto an optical carrier [49]. Building a terahertz-referenced signal from three coherent lasers

avoids this duplication stage and allows transmission over long distances through optical fibers. Independently of the frequency range of the reference transition, the demonstration that a narrow line can be produced in a mesoscopic sample by use of a Doppler-free technique opens the route to its implementation for a large variety of atomic systems.

ACKNOWLEDGMENTS

This work was financially supported by Labex FIRST-TF (Grant No. ANR-10-LABX-48-01), the A*MIDEX project (Grant No. ANR-11-IDEX-0001-02), and EquipEx Refimeve+ (Grant No. ANR-11-EQPX-0039), all funded by the Investissements d’Avenir French Government program managed by the French National Research Agency (ANR). Funding from CNES (Contract No. 151084) and Région Provence-Alpes-Côte d’Azur is acknowledged. M.C. acknowledges FIRST-TF for funding and a stimulating scientific environment, C. Chatou acknowledges financial support from CNES and Région Provence-Alpes-Côte d’Azur.

APPENDIX: CONDITIONS FOR A THREE-PHOTON DARK RESONANCE

The condition for a three-photon dark resonance implying a weak quadrupole transition in Ca^+ is better explained in the dressed-state picture, where the system of interest is a motionless atom represented by its quantized internal states plus n_B photons at 397 nm (energy $n_B \times \hbar\omega_B$), n_R photons at 866 nm (energy $n_R \times \hbar\omega_R$), and n_C photons at 729 nm (energy $n_C \times \hbar\omega_C$) [see Fig. 1(a) for the level scheme]. The three atom-laser interactions are characterized by their Rabi frequencies Ω_B , Ω_R , Ω_C , which are linear with the local laser electric field whatever the nature of the interaction. The eigenvalues of the noncoupled Hamiltonian depend on each laser detuning, which is defined as $\Delta_B = \omega_B - \omega_{P_{1/2}S_{1/2}}$, $\Delta_R = \omega_R - \omega_{P_{1/2}D_{3/2}}$, and $\Delta_C = \omega_C - \omega_{D_{5/2}S_{1/2}}$, where $\omega_{P_{1/2}S_{1/2}}$, $\omega_{P_{1/2}D_{3/2}}$, and $\omega_{D_{5/2}S_{1/2}}$ are the atomic transition frequencies. As further explained in Ref. [15], the dressed laser-coupled subsystem $\{(S_{1/2}, n_B, n_R, n_C), (D_{5/2}, n_B, n_R, n_C - 1)\}$ can be diagonalized at the lowest order of the perturbation and the new eigenstates $\{|S\rangle, |Q\rangle\}$ are then a coherent superposition of the two uncoupled states. $|S\rangle$ and $|Q\rangle$ are both coupled to the $|P\rangle$ state $(P_{1/2}, n_B - 1, n_R, n_C)$ through the strong dipole transition excited by the 397-nm laser, but with a very different strength, depending on the detuning Δ_C and the Rabi frequency Ω_C , which control the proportion of the two uncoupled states in the new eigenstates. Including $|D\rangle = (D_{3/2}, n_B - 1, n_R + 1, n_C)$, the subsystem $\{|Q\rangle, |P\rangle, |D\rangle\}$ coupled by the two dipole transitions forms a Λ scheme where the two feet are stable or metastable. This scheme is the paradigm of the configurations giving rise to a coherent population trapping in a dark state when the two (meta)stable states are degenerate in the

dressed-state picture [1]. Because the Λ scheme was built by first diagonalizing one of the interactions, this resonance condition implies here not two but three photons and is expressed as

$$\Delta_R = \Delta_B - \Delta_C - \delta_C, \quad (\text{A1})$$

where δ_C is the light shift induced by the quadrupole coupling on the 729-nm transition [15]. The laser couplings in the effective Λ scheme are Ω_R and $\alpha_C \Omega_B$, where $\alpha_C = \Omega_C / 2\Delta_C$ is the mixing coefficient induced by the quadrupole coupling.

- [1] E. Arimondo, *Coherent Population Trapping in Laser Spectroscopy* (Elsevier, 1996), p. 257.
- [2] G. Alzetta, A. Gozzini, L. Moi, and G. Orriols, An experimental method for the observation of r.f. transitions and laser beat resonances in oriented Na vapour, *Il Nuovo Cimento B (1971–1996)* **36**, 5 (1976).
- [3] O. Schmidt, R. Wynands, Z. Hussein, and D. Meschede, Steep dispersion and group velocity below $c/3000$ in coherent population trapping, *Phys. Rev. A* **53**, R27 (1996).
- [4] A. Nagel, L. Graf, A. Naumov, E. Mariotti, V. Biancalana, D. Meschede, and R. Wynands, Experimental realization of coherent dark-state magnetometers, *Europhys. Lett.* **44**, 31 (1998).
- [5] Peter D. D. Schwindt, Svenja Knappe, Vishal Shah, Leo Hollberg, John Kitching, Li-Anne Liew, and John Moreland, Chip-scale atomic magnetometer, *Appl. Phys. Lett.* **85**, 6409 (2004).
- [6] N. Cyr, M. Tetu, and M. Breton, All-optical microwave frequency standard: A proposal, *IEEE Trans. Instrum. Meas.* **42**, 640 (1993).
- [7] R. Wynands and A. Nagel, Precision spectroscopy with coherent dark states, *Appl. Phys. B* **68**, 1 (1999).
- [8] J. Vanier, Atomic clocks based on coherent population trapping: A review, *Appl. Phys. B* **81**, 421 (2005).
- [9] Peter Yun, François Tricot, Claudio Eligio Calosso, Salvatore Micalizio, Bruno François, Rodolphe Boudot, Stéphane Guérardel, and Emeric de Clercq, High-performance Coherent Population Trapping Clock with Polarization Modulation, *Phys. Rev. Appl.* **7**, 014018 (2017).
- [10] Moustafa Abdel Hafiz, Grgoire Coget, Peter Yun, Stéphane Gurandel, Emeric de Clercq, and Rodolphe Boudot, A high-performance Raman-Ramsey Cs vapor cell atomic clock, *J. Appl. Phys.* **121**, 104903 (2017).
- [11] Xiaochi Liu, Eugene Ivanov, Valeriy I. Yudin, John Kitching, and Elizabeth A. Donley, Low-drift Coherent Population Trapping Clock Based on Laser-cooled Atoms and High-coherence Excitation Fields, *Phys. Rev. Appl.* **8**, 054001 (2017).
- [12] R. H. Dicke, The effect of collisions upon the Doppler width of spectral lines, *Phys. Rev.* **89**, 472 (1953).
- [13] J. Kitching, S. Knappe, and L. Hollberg, Miniature vapor-cell atomic-frequency references, *Appl. Phys. Lett.* **81**, 553 (2002).

- [14] P. R. Hemmer, M. S. Shahriar, V. D. Natoli, and S. Ezekiel, AC-Stark shifts in a two-zone Raman interaction, *J. Opt. Soc. Am. B* **6**, 1519 (1989).
- [15] Caroline Champenois, Giovanna Morigi, and Jurgen Eschner, Quantum coherence and population trapping in three-photon processes, *Phys. Rev. A* **74**, 053404 (2006).
- [16] G. Grynberg, F. Biraben, M. Bassini, and B. Cagnac, Three-photon Doppler-free Spectroscopy: Experimental Evidence, *Phys. Rev. Lett.* **37**, 283 (1976).
- [17] Tao Hong, Claire Cramer, Warren Nagourney, and E. N. Fortson, Optical Clocks Based on Ultranarrow Three-photon Resonances in Alkaline Earth Atoms, *Phys. Rev. Lett.* **94**, 050801 (2005).
- [18] C. Champenois, G. Hagel, M. Houssin, M. Knoop, C. Zumsteg, and F. Vedel, Terahertz Frequency Standard Based on Three-photon Coherent Population Trapping, *Phys. Rev. Lett.* **99**, 013001 (2007).
- [19] I. I. Ryabtsev, I. I. Beterov, D. B. Tretyakov, V. M. Entin, and E. A. Yakshina, Doppler- and recoil-free laser excitation of Rydberg states via three-photon transitions, *Phys. Rev. A* **84**, 053409 (2011).
- [20] D. S. Barker, N. C. Pisenti, B. J. Reschovsky, and G. K. Campbell, Three-photon process for producing a degenerate gas of metastable alkaline-earth-metal atoms, *Phys. Rev. A* **93**, 053417 (2016).
- [21] Nils Scharnhorst, Jannes B. Wübbena, Stephan Hannig, Cornelius Jakobsen, Johannes Kramer, Ian D. Leroux, and Piet O. Schmidt, High-bandwidth transfer of phase stability through a fiber frequency comb, *Opt. Express* **23**, 19771 (2015).
- [22] Mathieu Collombon, Gaëtan Hagel, Cyril Chatou, Didier Guyomarc'h, Didier Ferrand, Marie Houssin, Caroline Champenois, and Martina Knoop, Phase transfer between three visible lasers for coherent population trapping, *Opt. Lett.* **44**, 859 (2019).
- [23] Michael Ramm, Thaned Pruttivarasin, Mark Kokish, Ishan Talukdar, and Hartmut Häffner, Precision Measurement Method for Branching Fractions of Excited $P_{1/2}$ States Applied to $^{40}\text{Ca}^+$, *Phys. Rev. Lett.* **111**, 023004 (2013).
- [24] M. Knoop, C. Champenois, G. Hagel, M. Houssin, C. Lisowski, M. Vedel, and F. Vedel, Metastable lifetimes from electron-shelving measurements with ion clouds and single ions, *Eur. Phys. J. D* **29**, 163 (2004).
- [25] Rekishu Yamazaki, Hideyuki Sawamura, Kenji Toyoda, and Shinji Urabe, Stimulated Raman spectroscopy and the determination of the D -fine-structure level separation in $^{40}\text{Ca}^+$, *Phys. Rev. A* **77**, 012508 (2008).
- [26] C. Solaro, S. Meyer, K. Fisher, M. V. DePalatis, and M. Drewsen, Direct Frequency-comb-driven Raman Transitions in the Terahertz Range, *Phys. Rev. Lett.* **120**, 253601 (2018).
- [27] C. Champenois, J. Pedregosa-Gutierrez, M. Marciante, D. Guyomarc'h, M. Houssin, and M. Knoop, A double ion trap for large coulomb crystals, *AIP Conf. Proc.* **1521**, 210 (2013).
- [28] M. R. Kamsap, J. Pedregosa-Gutierrez, C. Champenois, D. Guyomarc'h, M. Houssin, and M. Knoop, Fast and efficient transport of large ion clouds, *Phys. Rev. A* **92**, 043416 (2015).
- [29] J. Pedregosa, C. Champenois, M. Houssin, and M. Knoop, Anharmonic contributions in real rf linear quadrupole traps, *Int. J. Mass Spec.* **290**, 100 (2010).
- [30] M. Drewsen, C. Brodersen, L. Hornekær, J. S. Hangst, and J. P. Schiffer, Large ion Crystals in a Linear Paul Trap, *Phys. Rev. Lett.* **81**, 2878 (1998).
- [31] Leaf Turner, Collective effects on equilibria of trapped charged plasmas, *Phys. Fluids* **30**, 3196 (1987).
- [32] L. Hornekær and M. Drewsen, Formation process of large ion coulomb crystals in linear Paul traps, *Phys. Rev. A* **66**, 013412 (2002).
- [33] J. E. Thomas, S. Ezekiel, C. C. Leiby, R. H. Picard, and C. R. Willis, Ultrahigh-resolution spectroscopy and frequency standards in the microwave and far-infrared regions using optical lasers, *Opt. Lett.* **6**, 298 (1981).
- [34] S. Brandt, A. Nagel, R. Wynands, and D. Meschede, Buffer-gas-induced linewidth reduction of coherent dark resonances to below 50 Hz, *Phys. Rev. A* **56**, R1063 (1997).
- [35] Warren Nagourney, Jon Sandberg, and Hans Dehmelt, Shelved Optical Electron Amplifier: Observation of Quantum Jumps, *Phys. Rev. Lett.* **56**, 2797 (1986).
- [36] D. J. Larson, J. C. Bergquist, J. J. Bollinger, Wayne M. Itano, and D. J. Wineland, Sympathetic Cooling of Trapped Ions: A Laser-cooled Two-species Nonneutral ion Plasma, *Phys. Rev. Lett.* **57**, 70 (1986).
- [37] I. Sobelman, *Atomic Spectra and Radiative Transitions* (Springer-Verlag, Berlin, Heidelberg, New-York, 1992).
- [38] Florian Gebert, Yong Wan, Fabian Wolf, Christopher N. Angstmann, Julian C. Berengut, and Piet O. Schmidt, Precision Isotope Shift Measurements in Calcium Ions Using Quantum Logic Detection Schemes, *Phys. Rev. Lett.* **115**, 053003 (2015).
- [39] Thomas Zanon-Willette, Emeric de Clercq, and Ennio Arimondo, Ultrahigh-resolution spectroscopy with atomic or molecular dark resonances: Exact steady-state line shapes and asymptotic profiles in the adiabatic pulsed regime, *Phys. Rev. A* **84**, 062502 (2011).
- [40] J. W. Pollock, V. I. Yudin, M. Shuker, M. Yu. Basalaev, A. V. Taichenachev, X. Liu, J. Kitching, and E. A. Donley, ac stark shifts of dark resonances probed with Ramsay spectroscopy, *Phys. Rev. A* **98**, 053424 (2018).
- [41] A. Nagel, S. Brandt, D. Meschede, and R. Wynands, Light shift of coherent population trapping resonances, *Europhys. Lett.* **48**, 385 (1999).
- [42] S. Alighanbari, M. G. Hansen, V. I. Korobov, and S. Schiller, Rotational spectroscopy of cold and trapped molecular ions in the Lamb–Dicke regime, *Nat. Phys.* **14**, 555 (2018).
- [43] Kyle Arnold, Elnur Hajiyev, Eduardo Paez, Chern Hui Lee, M. D. Barrett, and John Bollinger, Prospects for atomic clocks based on large ion crystals, *Phys. Rev. A* **92**, 032108 (2015).
- [44] K. J. Arnold and M. D. Barrett, Suppression of Clock Shifts at Magnetic-field-insensitive Transitions, *Phys. Rev. Lett.* **117**, 160802 (2016).
- [45] J. Keller, T. Burgermeister, D. Kalincev, A. Didier, A. P. Kulosa, T. Nordmann, J. Kiethe, and T. E. Mehlstäubler, Controlling systematic frequency uncertainties at the 10^{-19} level in linear Coulomb crystals, *Phys. Rev. A* **99**, 013405 (2019).

- [46] Guoqing Hu, Tatsuya Mizuguchi, Xin Zhao, Takeo Minamikawa, Takahiko Mizuno, Yuli Yang, Cui Li, Ming Bai, Zheng Zheng, and Takeshi Yasui, Measurement of absolute frequency of continuous-wave terahertz radiation in real time using a free-running, dual-wavelength mode-locked, erbium-doped fibre laser, *Sci. Rep.* **7**, 42082 (2017).
- [47] T. Zanon-Willette, V. I. Yudin, and A. V. Taichenachev, Generalized hyper-Ramsay resonance with separated oscillating fields, *Phys. Rev. A* **92**, 023416 (2015).
- [48] Moustafa Abdel Hafiz, Grégoire Coget, Michael Petersen, Cyrus Rocher, Stéphane Guérardel, Thomas Zanon-Willette, Émeric de Clercq, and Rodolphe Boudot, Toward a High-stability Coherent Population Trapping Cs Vapor-cell Atomic Clock Using Autobalanced Ramsay Spectroscopy, *Phys. Rev. Appl.* **9**, 064002 (2018).
- [49] Shigeo Nagano, Motohiro Kumagai, Hiroyuki Ito, Masatoshi Kajita, and Yuko Hanado, Phase-coherent transfer and retrieval of terahertz frequency standard over 20 km optical fiber with 4×10^{-18} accuracy, *Appl. Phys. Express* **10**, 012502 (2017).